




Article

Dry Reforming of Methane Using a Swirl-Induced Plasma Discharge Reactor

R. Bharathi Raja ¹, Anusha C. Halageri ¹, R. Sankar ¹, Ramanujam Sarathi ² and Ravikrishnan Vinu ^{1,*}¹ Department of Chemical Engineering, Indian Institute of Technology Madras, Chennai 600036, India² Department of Electrical Engineering, Indian Institute of Technology Madras, Chennai 600036, India

* Correspondence: vinu@iitm.ac.in; Tel.: +91-44-22574187

Abstract: This study reports the dry reforming of methane (DRM) using non-thermal plasma in a swirl-induced point-plane electrode discharge reactor to produce syngas. This reactor geometry facilitates better mixing of the reactant gases in the plasma region, thus increasing the residence time and conversion of the reactants. The effect of varying flow rates and compositions of CO₂/CH₄ (v%/v%) on conversion was studied. A high-voltage AC power input of 50 W and 70 W at a frequency of 19 kHz was provided. The voltage–current characteristics with respect to time were studied. The results show that with an increase in the flow rate of the gas mixture from 0.5 to 2 LPM the conversion of both CO₂ and CH₄ decreases, while an increase in the concentration of CO₂ or CH₄ (from 25 to 75%) increases the conversion of the respective reactant. The products, viz. syngas (CO and H₂), C₂ hydrocarbons, and solid carbon, were characterized and quantified. The maximum total conversion of 44% was obtained for a CO₂:CH₄ ratio of 25:75 (v%/v%) at a flow rate of 0.5 LPM. The solid carbon collected from the reactor walls was analyzed, and it was found to be 89.9% pure with traces of oxygen functionality. The increase in flow rate decreased the specific energy input, which eventually resulted in lowering the energy cost.

Keywords: dry reforming of methane; non-thermal plasma; point-plane electrode discharge reactor; hydrogen; syngas



Citation: Raja, R.B.; Halageri, A.C.; Sankar, R.; Sarathi, R.; Vinu, R. Dry Reforming of Methane Using a Swirl-Induced Plasma Discharge Reactor. *Energies* **2023**, *16*, 1823. <https://doi.org/10.3390/en16041823>

Academic Editor: Alberto Abánades

Received: 1 December 2022

Revised: 18 January 2023

Accepted: 1 February 2023

Published: 12 February 2023



Copyright: © 2023 by the authors. Licensee MDPI, Basel, Switzerland. This article is an open access article distributed under the terms and conditions of the Creative Commons Attribution (CC BY) license (<https://creativecommons.org/licenses/by/4.0/>).

1. Introduction

Owing to increasing concerns about climate change, technologies are emerging to mitigate the ill effects of the increased emission of greenhouse gases (GHGs). Although fossil fuels stand ahead in the order of sources of GHG emissions, recently it has been reported that renewable sources of energy also contribute to the emission of GHGs [1]. The life cycle GHG emission from waste treatment alone amounts to 1000 g CO₂eq/kWh [1]. Thermochemical treatment of renewable and waste feedstocks such as biomass, waste plastics, and municipal solid wastes contain CH₄ and CO₂ as the major gaseous components.

Several methods have been developed to convert the two major greenhouse gases, methane (CH₄) and carbon dioxide (CO₂), into valuable products independently. Dry reforming of methane, in a single reaction, converts both these gases into valuable fuel and chemical feedstock such as carbon monoxide (CO) and hydrogen (H₂). Hence, it is gaining more attention. Dry reforming of methane (DRM) is an endothermic process that requires high temperatures (above 800 °C) to attain reasonable, energy-efficient, and cost-effective conversion of the highly stable CO₂ and CH₄ mixture. The complete conversion of CH₄ and CO₂ takes place beyond 900 °C [2]. The thermochemical DRM process requires a catalyst to operate under reduced temperatures. Ekeoma et al. [3] reviewed studies on silica-supported Ni-based catalysts for DRM that showed significant conversions of CH₄ and CO₂ (>50%). Albarazi et al. [4] utilized ceria–zirconia-doped Ni/SBA-15 catalysts, and achieved 61% and 68% conversions of CH₄ and CO₂, respectively. A major drawback of the DRM process using heterogeneous catalysts is coke formation, which limits the long-term stability,

activity, and usability of the catalyst [5]. The use of catalysts with high lattice oxygen and oxygen defects is shown to minimize carbon deposition and improve stability. Key innovations in rational catalyst design including multi-metal catalysts with mixed oxide support and promoters in the mesoporous range are required for thermochemical DRM to demonstrate the economic viability of the process for long-term on-stream operation.

The various methods of production, storage, and applications of hydrogen are reviewed by Qureshi et al. [6] and Pudukudy et al. [7]. It is evident that steam methane reforming is the only developed technology that generates the maximum amount of H₂ generated in the world (40–50 million tons per year). However, owing to the CO₂ emissions from this process, other technologies are gaining importance in recent times to generate hydrogen with lower or zero emission of CO₂. In this regard, methane cracking or methane pyrolysis generates H₂ with zero CO₂ emission, while generating solid carbon as a valuable byproduct. DRM can also be viewed as a H₂ and carbon generation process, while simultaneously utilizing CO₂. On the other hand, biogas production from biodegradable wastes, biomass, and municipal solid wastes is gaining importance from a solid waste management viewpoint. Biogas, which is a mixture of CH₄ and CO₂, can be used for distributed power generation. Biogas can also be converted to bio-CNG containing ~95% methane. However, the separation and sequestration of CO₂ from biogas is a major concern. This brings DRM to the spotlight for direct conversion of the mixture of CO₂ and CH₄ to syngas and fuels. Parsapur et al. [8] showed that DRM requires significant input energy of 1143 kJ/mol_{CH₄}, whereas steam reforming of methane requires 1098 kJ/mol_{CH₄} for producing syngas. Altogether, DRM should be viewed as a CO₂ utilization process. The existing perspective can be changed by using plasma technology, where energy efficiency can be improved significantly with better control of the process operation along with efficient recovery of carbon byproducts. More importantly, the process becomes energy efficient when renewable electricity is used for its operation.

Plasma can be described as a region of ionized gas with balanced charges of positive ions and electrons, radicals, and neutral molecules. This region is highly interactive, electrically conductive, and responds to electromagnetic fields. When a neutral gas molecule is energized, the molecules are excited to a higher energy state. With more energy supply, the molecules attain higher energy levels such that they overcome the bond dissociation energy to become ions and electrons. This state is called plasma. If the energy provided is in the form of heat, then it is called thermal plasma (TP), wherein all the molecules are near the local thermodynamic equilibrium (LTE), i.e., $T_e = T_{\text{heavy}}$. Therefore, it is also called equilibrium plasma. On the other hand, if the energy provided is electrical energy, then it is called non-thermal plasma (NTP). It is also called non-equilibrium plasma because the molecules do not attain LTE ($T_e \gg T_{\text{heavy}}$). There are different types of NTPs, namely dielectric barrier discharge (DBD) plasma, microwave (MW) plasma, gliding arc discharge (GAD), radiofrequency (RF) discharge, corona discharge, and glow discharge [9,10]. Non-thermal plasma is highly advantageous owing to its ability to produce high thermal energy to initiate a chemical reaction at temperatures as low as room temperature.

DRM was investigated using a thermal torch with nitrogen as carrier gas and a discharge power of 9.6 kW along with a water-cooling system [11]. The maximum conversion of 88% of CH₄ and 70% of CO₂ is reported at a 2:3 molar ratio of CH₄:CO₂. Evidently, the thermal plasma for DRM involves high flow rates of carrier gases, which is usually greater than that of the working gas, along with auxiliary cooling systems to attain high conversions. Hence, the benefits of a high conversion rate in thermal plasma reactors come with questionable energy efficiency and energy costs. Integrating such a high-power-demanding thermal plasma process with sustainable electricity is therefore an option to be considered. DRM using DBD along with the synergetic effect of a catalyst has been studied extensively and is shown to be well-suited for chemical energy storage systems [12]. An investigation of the DRM in DBD was performed, and the study achieved a maximum total conversion of 84% with an energy efficiency of 8.5% at CO₂:CH₄ ratio of 90:10 (v%/v%). However, the drawback of the DBD process is its low energy efficiency, which is lesser than 10% [13].

Raja et al. [14] used a double DBD reactor for DRM and achieved a CO₂ conversion of 10% at a CH₄:CO₂ ratio of 50:50 (v%/v%) with a specific energy input of 53.8 kJ/L. Another study reported a total conversion of CH₄ and CO₂ up to 28% by varying the size, and with α -Al₂O₃ as dielectric packing material [15]. Different catalytic materials were integrated into the DBD reactors, and an energy efficiency of 4.4% was achieved. The maximum conversion of CO₂ and CH₄ were 32% and 22%, respectively, using a CO₂:CH₄ ratio of 50:50 (v%/v%) [16]. The authors developed a novel gas inlet parallel plate DBD configuration and obtained a total conversion of 19.2% with an energy cost of 1.17 kWh mol⁻¹ [17]. Nonetheless, the DBD reactors for DRM need improvement in energy efficiency, which can be achieved by altering the reactor configuration and suitable catalysts.

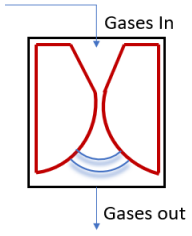
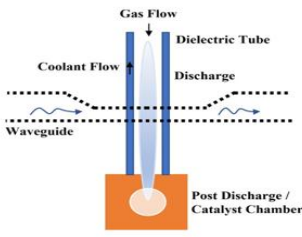
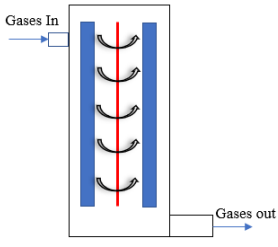
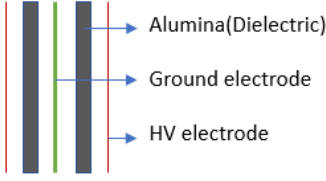
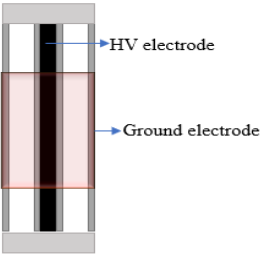
A study on DRM in microwave plasma reported a conversion of 68.4% for CO₂ and 96.8% for CH₄ at a CO₂:CH₄ ratio of 50:50 (v%/v%). The reforming was done at atmospheric pressure and 6 kW of plasma power. This shows that the conversion of CO₂ and CH₄ through microwave plasma requires high energy input and low operating pressures, which can be a drawback for scaling up the process for industrial applications [18]. A knife-shaped gliding arc discharge (GAD) for DRM using a high-frequency AC power supply was developed, and reasonable CH₄ and CO₂ conversions of 58.8% and 53.2%, respectively, were reported. GAD can be used in thermal and non-thermal regimes. Combining the advantages of both regimes can be effective for gas conversions. The inherent disadvantage of GAD is the high current at the shortest gaps, which can result in electrode erosions. Moreover, due to the 2D structure, not all the gases are effectively converted [19]. To overcome this problem, some newly developed three-dimensional (3D) rotating arc discharges have been reported in the literature for CO₂ and CH₄ conversion. A method of creating forward and reverse vortex flow in a gliding arc plasmatron (GAP) was proposed by Nunnally et al. [20], wherein the discharges are produced by applying both AC and DC. Another work reported GAP in a reversed vortex flow, and investigated the effect of N₂ addition on CO₂ dissociation [21]. An extensive study on DRM, and the effect of real gas mixtures by adding N₂ and O₂ in GAP has been carried out by Bogaerts and co-workers [22,23]. Table 1 presents a summary of the reactor configurations reported for DRM along with the conversion and energy efficiencies.

The combined advantages of gliding and rotating arc discharges in a tangential flow rotating gliding arc reactor with the synergetic effect of Lorentz force were used for CO₂ activation [24]. Raja et al. [25] developed a swirl-induced rotating glow discharge reactor for CO₂ conversion and studied the fluid and discharge dynamics. Higher conversion with low specific energy input was reported in the laminar regime. A swirl-induced point-plane discharge reactor was developed for studying the pyrolysis of methane, and the highest conversion of 19.7% was obtained at a flow rate of 0.5 L/min and input power of 55 W [26]. One of the key advantages of plasma technology is the ability to seamlessly control the process by switching on/off the electrical power input to the reactor [12]. Therefore, combining this process with a renewable electricity source has the potential of producing environmentally friendly fuels and value-added chemicals.

In this study, a non-thermal plasma reactor with a newly developed point-plane electrode configuration is used for the DRM. The injection of reactant gases through the guided vanes incorporated in the plane electrode ensures the swirling motion of the gas molecules, which results in central toroidal recirculation zones. This particularly increases the residence time and mixing of the gas molecules, and eventually aids in improving the conversion at a lower energy cost. More importantly, this study employs the reactant gases without any dilution. Many studies in the literature have employed inert diluent gases such as nitrogen or argon to improve the conversion. However, in order to demonstrate the practical applicability of the process wherein the separation of the inert gas from the product gas mixture will be an issue, no inert gas is used. Experiments at four different flow rates in the range of 0.5–2 L per minute (LPM) and varying CO₂:CH₄ ratios of 50:50, 75:25, and 25:75 (v%/v%) were performed. The conversion, yield, and product distribution

were studied, and the characterization of carbon deposits was performed to determine the size and purity.

Table 1. Reactor configurations reported for DRM and the corresponding conversion and energy efficiencies.

S. No.	Reactor Configuration	Reactor Type	Power Supply Type	Conversion (%) of CH ₄ and CO ₂ at corresponding CH ₄ :CO ₂ Ratio (v%/v%)	Maximum Energy Efficiency	References
1.		Knife-shaped Gliding arc plasmatron	High-frequency AC source	58.8, 52.3 at 40:60	2.21 mmol/kJ	Xia et al. (2017) [18]
2.		Microwave Plasma Torch	Not Specified	68.4, 96.8 at 50:50	Not reported	Chun et al. (2017) [17]
3.		Cylindrical Gliding arc plasmatron	DC High voltage	10, 18 at 25:75	66%	Cleiren et al. (2017) [21]
4.		Coaxial DBD with alumina as dielectric	DC High voltage	33, 22 at 50:50	4%	Andersen et al. (2020) [15]
5.		Double DBD reactor	AC high voltage	CO ₂ –10.1 at 50:50	53.8 kJ/L	Raja et al. (2020) [14]

2. Materials and Methods

Experimental Setup and Working

Figure 1a shows the schematic of the experimental setup employed for DRM. The plasma discharge is generated in the electrode hub, whose schematic is depicted in Figure 1b. The point-plane electrode arrangement consists of a tungsten (WT20) electrode of 6 mm diameter with a sharp tip that is positioned 16 mm from the swirl electrode's central hub.

The swirl electrode or swirl injector has eight guided vanes positioned at 45° . This ensures a swirl number of 0.9, which is shown to result in the formation of recirculation zones. These vanes are mounted on a central hub of diameter 20 mm. The detailed design of the swirl electrode is given in Raja et al. [25], and the point-plane electrode configuration is given in our recent report on methane pyrolysis using this reactor [26]. Figure 1c shows the snapshots of the reactor section and the electrodes. The schematic of the electrodes in Figure 1b is shown in an upside-down configuration to elucidate the swirl vane geometry. However, in the actual setup, the gases exit the swirl electrode from the top, and the plasma is established between the electrodes.

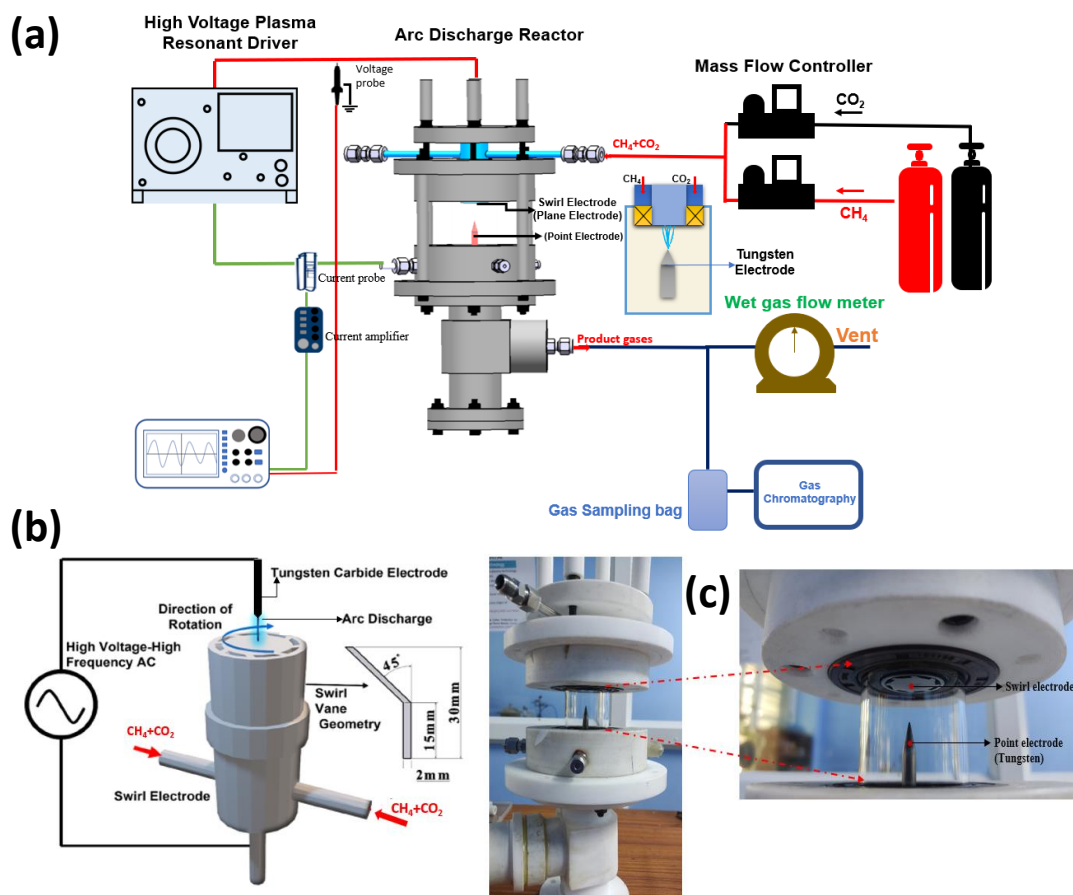


Figure 1. (a) Schematic of the experimental setup. (b) Schematic of the point-plane electrode. (c) Snapshots of the setup and the point-plane electrodes.

When the reactant gas, a mixture of CH_4 and CO_2 , enters through the guided vanes, they attain a swirl motion creating pressure gradients along the axial and radial directions of the flow, resulting in a central recirculation zone (CRZ). Recirculation of the reactant gas mixture in the plasma region offers higher residence time and mixing time for the reaction. The device provides a high power input at the maintained frequency. As depicted in the schematic, Figure 1a, the flow rates of the reactant gases, CO_2 and CH_4 , are controlled individually by two mass flow controllers, and the gases are mixed in a mixing chamber of 5 L capacity. The gases enter the reactor through the swirl injector. A high-voltage resonant driver with a minimum AC frequency of 19 kHz was used to generate plasma. The current and voltage were measured using a two-channel oscilloscope, a current probe along with an amplifier, and a voltage probe. The specifications of the plasma resonant driver, voltage probe, current probe, and oscilloscope are provided in Table 2.

Table 2. Details of the equipments and analytical facilities used in this study.

Equipment	Specification
Mass flow controller	Alicat MC-2SLPM
High Voltage (HV) Plasma resonant driver	PVM500, Information Unlimited
Voltage probe	Lecroy PPE 20 kV, 100 MHz
Current probe and amplifier	Tektronix TCP312A, 100 MHz, TCPA300
Oscilloscope	Tektronix TBS 1102B
Gas chromatography	Agilent 7820 GC Porapak-Q column (2 m, 80/100 mesh) Oven temperature—50 °C TCD and FID temperatures—200 and 260 °C, respectively Argon flow rate—10 mL/min
Elemental CHNS analysis	Thermo Flash 2000 (ASTM- D5291 method)
SEM-EDAX	Zeiss Evo-18
FTIR	Agilent Cary 630 4 cm ⁻¹ resolution, attenuated total reflectance (ATR) mode

A 5 µm filter was placed at the exit of the reactor to collect the carbon particles in the product stream. The volumetric flow rates of the gas mixture were recorded before and during the plasma discharge process using a wet gas flow meter installed downstream before the vent. A gas sampling bag of 2 L capacity was used to collect the gas for composition analysis using a gas chromatograph (GC). The carbon particles collected from the walls of the reactor were subjected to elemental CHNS analysis, scanning electron microscopy combined with energy-dispersive X-ray analysis (SEM-EDAX), and Fourier transform infrared (FTIR) spectroscopy to confirm the purity, morphology, and functional groups present in the sample. Table 2 presents the details of various instruments and analytical equipments used in this study.

The reactions were performed at four different flow rates, viz. 0.5, 1, 1.5, and 2 LPM, and with varying CO₂:CH₄ ratios, 50:50, 75:25, and 25:75 (v%/v%). This helps simulate the uncertain composition of the biogas generated in the landfills and via anaerobic digestion of biomass and solid wastes. The effect of power input was also investigated for an equal composition mixture of CO₂:CH₄ (50:50 v%/v%).

Table 3 [27,28] shows a summary of the electron impact reactions that occur during the DRM for the formation of CO and H₂. The possible backward reactions and other reactions that might occur during the process are also listed. As non-thermal plasma does not energize the bulk of the gas, a majority of the undesired reactions do not occur, thus minimizing the formation of the by-products. The conversion, yield, and energy cost were calculated using the following equations with a gas correction factor [29,30].

$$X_{\text{CO}_2/\text{CH}_4} = \frac{C_{\text{CO}_2/\text{CH}_4}^{\text{in}} - \alpha C_{\text{CO}_2/\text{CH}_4}^{\text{out}}}{C_{\text{CO}_2/\text{CH}_4}^{\text{in}}} \quad (1)$$

where $X_{\text{CO}_2/\text{CH}_4}$ denotes the conversion of CO₂ or CH₄, $C_{\text{CO}_2/\text{CH}_4}^{\text{in}}$ and $C_{\text{CO}_2/\text{CH}_4}^{\text{out}}$ are inlet and outlet concentrations of CO₂ and CH₄, and α is the gas conversion factor defined as the ratio of the exit-to-entrance flow rate.

Table 3. Electron impact reactions taking place during the dry reforming of methane [27,28].

Reaction Type	Reaction	Number
Reactant conversion	$\text{CH}_4 + e \rightarrow \text{CH}_3 + \text{H} + e$	(R1)
	$\text{CH}_4 + e \rightarrow \text{CH}_2 + \text{H}_2 + e$	(R2)
	$\text{CH}_4 + e \rightarrow \text{CH} + \text{H} + \text{H}_2 + e$	(R3)
	$\text{CO}_2 + e \rightarrow \text{CO} + \text{O}$	(R4)
	$\text{CH}_4 + \text{O} \rightarrow \text{CH}_3 + \text{OH}$	(R5)
	$\text{CH}_4 + \text{OH} \rightarrow \text{CH}_3 + \text{H}_2\text{O}$	(R6)
	$\text{CH}_4 + \text{H} \rightarrow \text{CH}_3 + \text{H}_2$	(R7)
	$\text{CO}_2 + \text{H} \rightarrow \text{CO} + \text{OH}$	(R8)
	$\text{H} + \text{H} + \text{M} \rightarrow \text{H}_2 + \text{M}$	(R9)
Competing reactions	$\text{CH}_3 + \text{OH} \rightarrow \text{CH}_3\text{OH}$	(R10)
	$\text{CH}_3\text{OH} + \text{OH} \rightarrow \text{CH}_2\text{O} + \text{H} + \text{H}_2\text{O}$	(R11)
	$\text{CH}_3 + \text{O} \rightarrow \text{CH}_2\text{O} + \text{H}$	(R12)
	$\text{CH}_2\text{O} + \text{O} \rightarrow \text{CHO} + \text{OH}$	(R13)
	$\text{CH}_2\text{O} + \text{OH} \rightarrow \text{CHO} + \text{H}_2\text{O}$	(R14)
	$\text{CHO} + \text{OH} \rightarrow \text{CO} + \text{H}_2\text{O}$	(R15)
	$\text{CHO} + \text{O} \rightarrow \text{CO} + \text{OH}$	(R16)
Formation of reactants	$\text{CO} + \text{O} \rightarrow \text{CO}_2$	(R17)
	$\text{CO} + \text{OH} \rightarrow \text{CO}_2 + \text{H}$	(R18)
	$\text{CH}_3 + \text{H} \rightarrow \text{CH}_4$	(R19)
H ₂ consumption	$\text{H}_2 + \text{O} \rightarrow \text{OH} + \text{H}$	(R20)
	$\text{H}_2 + \text{OH} \rightarrow \text{H}_2\text{O} + \text{H}$	(R21)
Formation of C and C ₂ hydrocarbons	$e + \text{CH}_4 \rightarrow e + \text{C} + \text{H}_2$	(R22)
	$\text{CH}_4 + \text{CH} \rightarrow \text{C}_2\text{H}_4 + \text{H}$	(R23)
	$\text{C}_2\text{H}_5 + \text{H} \rightarrow \text{C}_2\text{H}_6$	(R24)

The total conversion X_{total} of DRM process is calculated as,

$$X_{total} = C_{\text{CO}_2}^{in} X_{\text{CO}_2} + C_{\text{CH}_4}^{in} X_{\text{CH}_4} \quad (2)$$

The specific energy input (SEI), is calculated as,

$$SEI(\text{kJ L}^{-1}) = \frac{\text{Power deposited (kW)}}{\text{Total flow rate (L min}^{-1})} \cdot 60 (\text{s min}^{-1}) \quad (3)$$

The energy cost (EC) is calculated using the following equation,

$$EC\left(\frac{\text{eV}}{\text{molecule}}\right) = \frac{SEI(\text{kJ L}^{-1}) \cdot V_{mol} \cdot a}{X_{total} \cdot N_A} \quad (4)$$

where Avagadro's number $N_A = 6.023 \times 10^{23} \text{ mol}^{-1}$, conversion factor $a = 6.24 \times 10^{21} \text{ eV kJ}^{-1}$, and $V_{mol} = 24.5 \text{ L mol}^{-1}$.

3. Results and Discussion

3.1. Electrical Characterization

The high-voltage pulses were kept at a minimum frequency of 19 kHz. At this frequency, the HV power supply exhibits the maximum power in relation to the applied voltage. The studies were conducted at two levels of power input based on resonant driver settings, viz., low-power and high-power modes. The combined characteristic of the reactor configuration and the plasma resonant driver exhibited 50 W and 70 W at low and high-power modes, respectively. In these modes, the amplitude of the applied voltage was fixed and a slight rise in current increased the overall power of the plasma discharge. The power measured is the total power consumed by the HV supply and the plasma reactor. The voltage and current waveforms shown in Figure 2 correspond to a plasma power of 40 W, which is due to the power losses in the resonant driver circuit. When the voltage across the electrode reaches 8.2 kV, the complete breakdown of the gas medium initiates the

sudden current rise. The voltage–current (V–I) profiles follow a repetitive pattern in every half cycle of the supply voltage providing sustained plasma generation. The turbulent flow of the gases in the reactor and the short-lived current discharge peak help to maintain a low temperature in the reactor. The maximum temperature observed during the process was 82 °C. The temperature profile inside the reactor along with the infrared images of the plasma reactor at the beginning of the experiment and at 30 min corresponding to the attainment of steady-state temperature are shown in Figure 3.

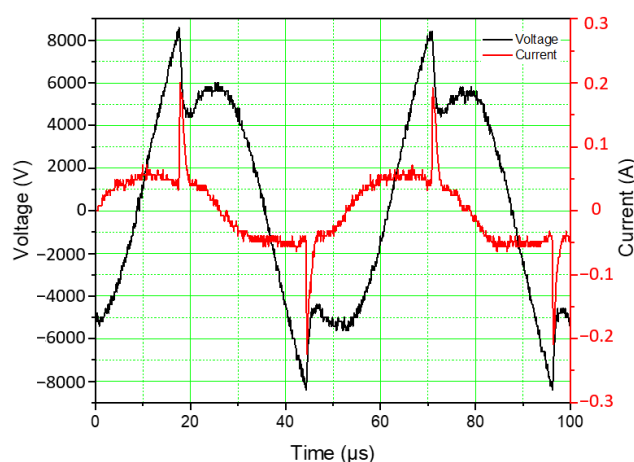


Figure 2. Discharge voltage and current profiles at a flow rate of 0.5 LPM with a CO₂:CH₄ ratio of 50:50 (v%/v%) for a timespan of 100 μs.

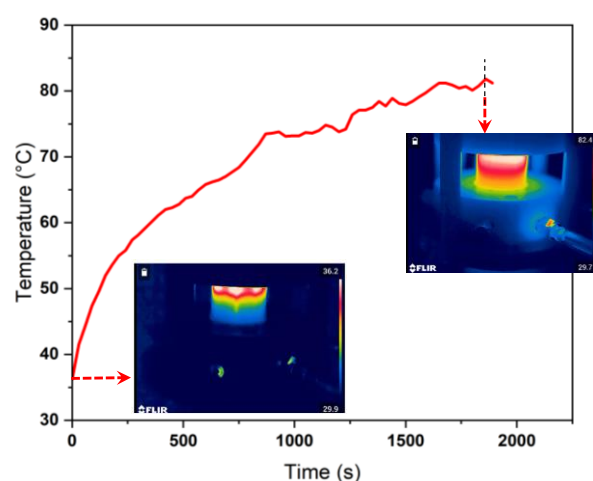


Figure 3. Temperature profile inside the reactor as measured by the infrared camera when a CH₄:CO₂ ratio of 75:25 (v%/v%) at 0.5 LPM was used. The snapshots of the reaction zone at 0 min and 30 min are depicted in the inset images.

3.2. Effect of Flow Rate on Conversion, Yield, and Energy Cost

The gas samples were collected after 25 min of plasma discharge and temperature stabilization. The effect of flow rate on CO₂ conversion is shown in Figure 4. In point-plane discharge configuration at 50 W input power, the conversion of CO₂ decreases with increasing flow rate. As the flow rate increases, due to increased velocity, the gas molecules flow past the plasma region within a short time period. However, lower flow rates offer increased residence time and recirculation, thus enhancing the conversion of CO₂. The SEI also decreases as the flow rates increase according to Equation (3). The SEI value decreased from 6 kJ/L (0.5 LPM) to 1.5 kJ/L (2 LPM) for all three concentrations of CO₂ (25%, 50%, and 75%) at an input power of 50 W. Owing to the aforementioned observations, the maximum CO₂ conversion of 23% was obtained at a CO₂:CH₄ ratio of 75:25 (v%/v%)

at 50 W and a flow rate of 0.5 LPM. The high conversion can also be due to the high concentration of CO₂ along with the low flow rate and high SEI. When the power input was increased to 70 W at 1 LPM for the equal composition mixture, the conversion of CO₂ increased significantly to 31% from 13% (at 50 W) with an increased SEI of 4.2 kJ/L. Similarly, at 2 LPM, the increase in CO₂ conversion was from 10% (at 50 W) to 15% (at 70 W). This is clearly due to higher energy deposition to the reactant molecules, which results in better conversion.

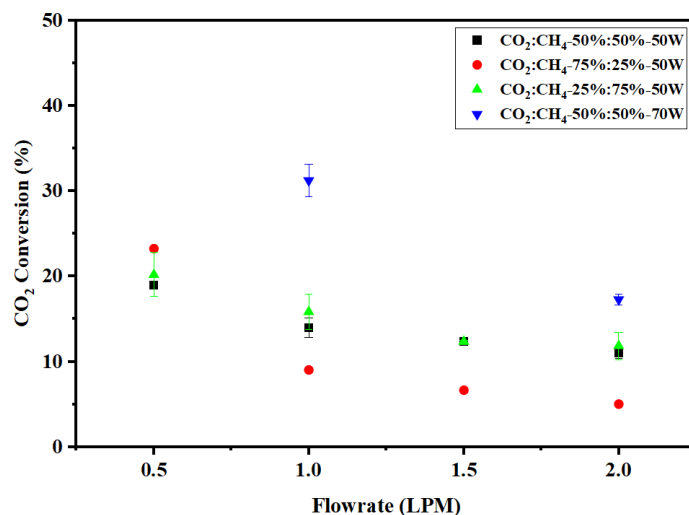


Figure 4. Effect of flow rate on CO₂ conversion.

The effect of flow rate on CH₄ conversion is shown in Figure 5. As in the case of CO₂, the maximum conversion of CH₄ of 52% is achieved at the lowest flow rate of 0.5 LPM for the CH₄-rich mixture (CO₂:CH₄ ratio of 25:75 (v%/v%)). The high concentration of CH₄ in the feed gas stream results in a better rate of conversion to H₂ and other products. Table 3 shows that the dissociation of CH₄ molecules takes place through an electron impact dissociation reaction. Thus, the conversion of CH₄ is always higher as compared to CO₂. The bond dissociation energy of the C–H bond in CH₄ (4.48 eV) is relatively low compared to C=O in CO₂ (5.52 eV) [21,25]. Owing to the high SEI, CH₄ conversion increased from 20% (at 50 W) to 31% (at 70 W). A similar increase was also observed at 2 LPM as evidenced in Figure 5. The electron impact dissociation of CH₄ forms CH₃ radicals and H atoms, and with subsequent removal of H atoms in a series of reactions, short-lived species such as CH₂ and CH are formed, and ultimately solid carbon is generated. Notably, carbon deposits were observed on the reactor walls as a result of CH₄ dissociation. As there was very little deposition of carbon particles found on the point electrode, the plasma was sustained for a longer time without arc extinction. This is in sharp contrast to our own study of methane pyrolysis using this reactor, where carbon channeling led to the extinction of the arc beyond 16 min of operation [26].

The effect of flow rate on the total conversion of the gaseous mixture is shown in Figure 6. Longer residence time at low flow rates increases the probability of electron impact dissociation and energy transfer to the molecules, thus resulting in better conversion. The graph shows a decreasing trend of conversion with an increasing flow rate. The maximum total conversion of 44% was achieved at 0.5 LPM with a CO₂:CH₄ ratio of 25:75 (v%/v%). This observation is in line with our earlier studies on CO₂ conversion to CO and CH₄ conversion to H₂ using swirl-induced discharge reactors, where high flow rates resulted in a lower conversion of the reactant gas [25,26]. As mentioned in Table 3, there are various reactions taking place that result in products other than H₂ and CO. Accordingly, the formation of C₂H₆ and C₂H₄ is quite favorable. Furthermore, C₂H₂ is formed in a series of free radicals and electron impact reactions. The C₂ hydrocarbon concentration in the product stream followed the trend: C₂H₂ > C₂H₄ > C₂H₆. The

maximum ethylene concentration was 0.35% and the maximum ethane concentration was 0.04% at a $\text{CO}_2:\text{CH}_4$ ratio of 25:75 (v%/v%). The effect of flow rate on gaseous product composition is shown in Figure 7. The maximum acetylene concentration was 3.6% at a $\text{CO}_2:\text{CH}_4$ ratio of 25:75 (v%/v%). This shows that increasing CH_4 content in DRM results in substantial C_2 hydrocarbon formation.

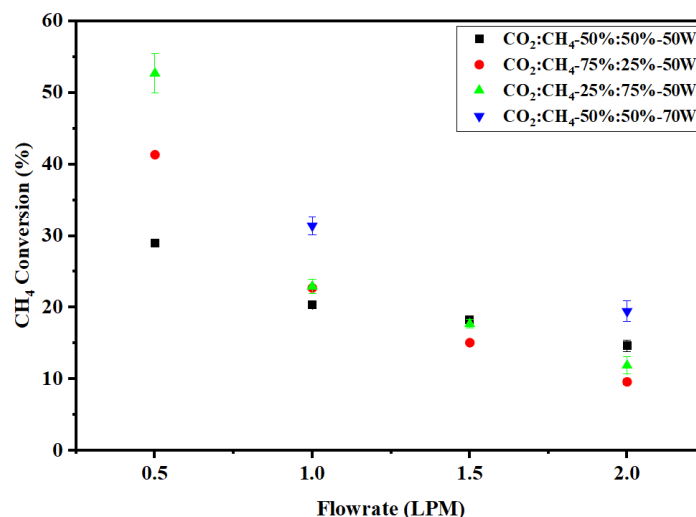


Figure 5. Effect of flow rate on CH_4 conversion.

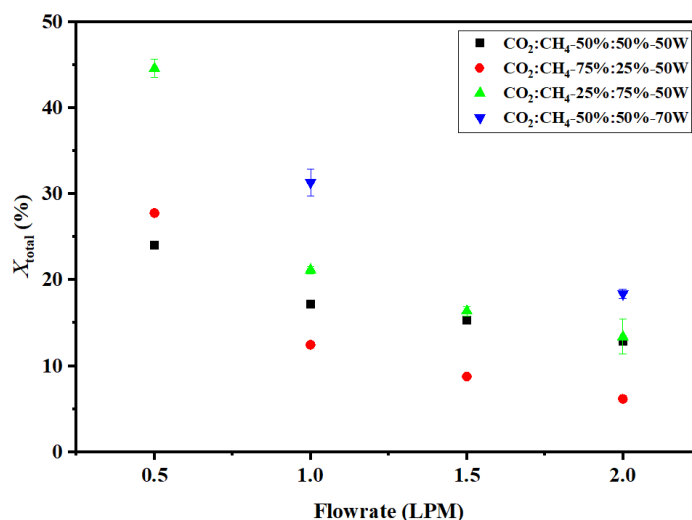


Figure 6. Effect of flow rate on total conversion.

The effect of flow rate on syngas yield is shown in Figure 8. The highest H_2 and CO yields were 31% and 24.7%, respectively, at 0.5 LPM and a $\text{CO}_2:\text{CH}_4$ ratio of 50:50 (v%/v%) (50 W). At a $\text{CO}_2:\text{CH}_4$ ratio of 50:50 (v%/v%) and a flow rate of 1 LPM, the H_2 and CO yields were 26.4% and 18.7%, respectively. As the flow rate increases, the yield decreases due to lower conversion. The experiments with 70 W power input resulted in a better yield than that at 50 W at both 1 LPM and 2 LPM flow rates. This shows that the yield can be tuned by varying the flow rate and power. It is also observed that by increasing either CO_2 or CH_4 concentration in the mixture, the yields of CO or H_2 are improved, respectively. Thus, the H_2/CO ratio can be varied by varying the concentrations of CO_2 and CH_4 in the DRM process. Maximum H_2/CO ratios of 5.5–6.0 were obtained at 1.5 and 2 LPM using a $\text{CO}_2:\text{CH}_4$ ratio of 25:75 (v%/v%). As shown in Table 3, the reaction of active species generated from CH_4 pyrolysis (such as H) with CO_2 generates OH species. Likewise, O generated from CO_2 interacts with CH_4 and CH_3 to form OH , and

in a series of reactions, CO is generated. H radicals are also generated through reactions R11, R12, and R18, which act as precursors for the formation of H₂. Thus, the formation of CO and H₂ also occurs through the interaction of the active species generated from the two co-reactants. The tracking of the intermediate species along with kinetic modeling of the reaction network will pave way for a better understanding of the tuning of product composition with different CO₂:CH₄ ratios.

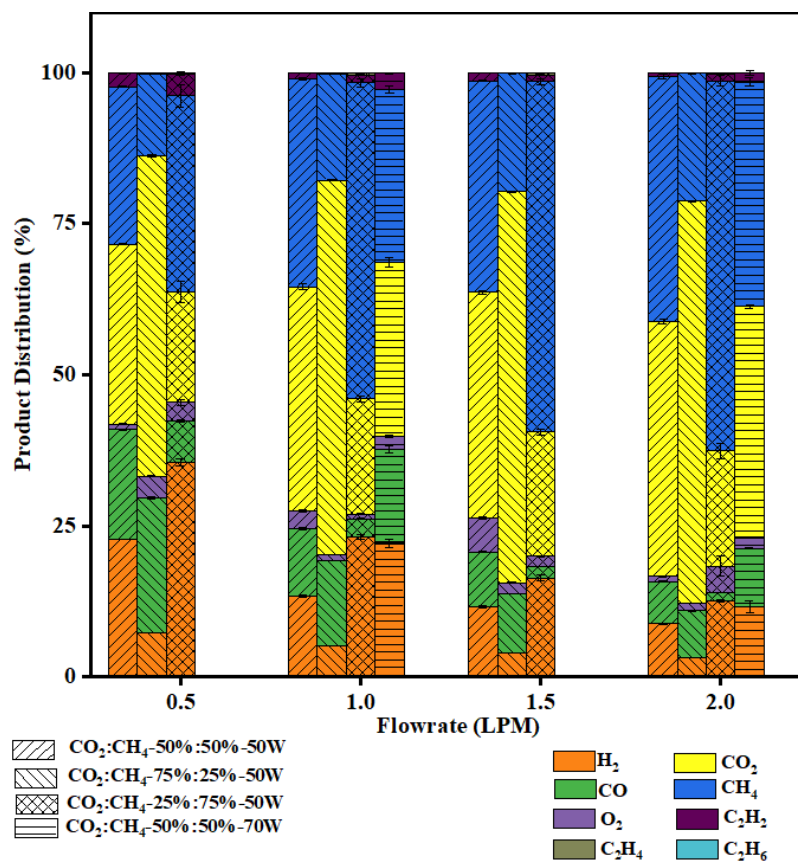


Figure 7. Effect of flow rate on gaseous product distribution.

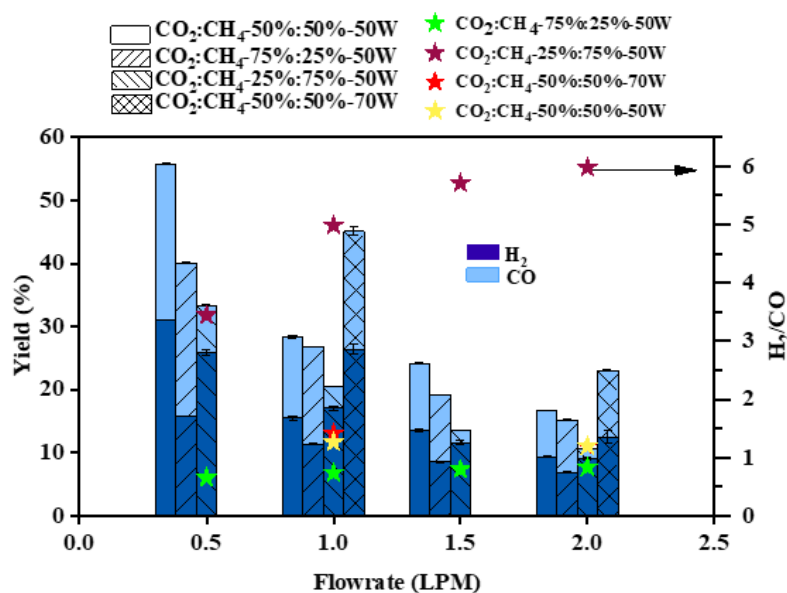


Figure 8. Effect of flow rate on H₂ and CO yield.

The effect of flow rate on energy cost (eV/molecule) is shown in Figure 9. The energy cost for a CO₂:CH₄ ratio of 50:50 (v%/v%) decreases from 6.3 to 3 (eV/molecule) as the flow rate increases from 0.5 to 2 LPM. The steady decrease is a direct impact of decreasing SEI with the flow rate. On the contrary, this trend was not observed for other mixture compositions and power, and the energy cost remains almost constant. This can be attributed to the fact that total conversion is proportional to SEI.

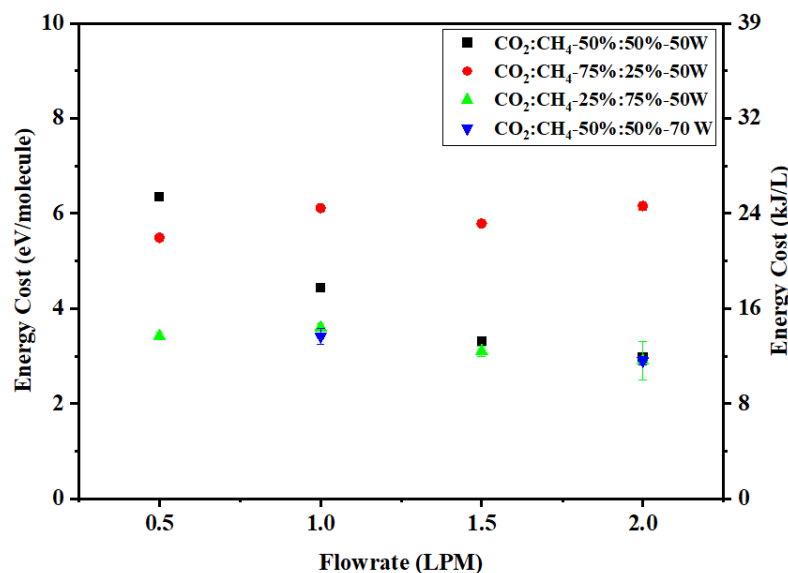


Figure 9. Effect of flow rate on energy cost.

Compared to the literature, the point-plane electrode configuration exhibits comparable conversion at a slightly higher energy cost. One study reported a maximum conversion of 18% and 10% for CO₂ and CH₄, respectively, using GAP with a CH₄ inlet concentration of 25%. The overall maximum energy cost for the highest conversion was 2.5 eV/molecule [22]. RGA co-driven by a magnetic field and tangential flow exhibited a maximum CO₂ and CH₄ conversion of 36% with an energy cost efficiency of 27.6% [27]. In another study on DRM using RGA, maximum methane conversion of ~45% corresponding to low SEI of ~20 kJ/L was obtained using 60:40 (v%/v%) of CH₄:CO₂ at 10 kV [31]. High SEI values were obtained only with CO₂-rich mixtures. When RGA was equipped with a dual DC power supply using argon as a carrier gas, CO₂ and CH₄ conversions of 12.8% and 10.9%, respectively, with an SEI of 6.7 kJ/L were reported [32]. The highest total conversion of 62% and lowest energy cost of 3.5 eV/molecule were reported for confined atmospheric pressure glow discharge [30].

3.3. Characterization of Carbon Particles

The particles collected from experiments performed using a methane-rich mixture (CO₂:CH₄ ratio of 25:75 v%/v%) were subjected to elemental CHNS analysis to evaluate the purity of carbon. The amounts of carbon and hydrogen were determined to be 89.9 wt% and 3.9 wt%, respectively. No sulfur or nitrogen was detected. Figure 10a shows the SEM images of carbon particles collected from the quartz wall. The images show two different morphologies. The smooth spherical morphology is interpreted as pure carbon, whereas the coarse structures are possibly due to oxygen on the surface of the carbon. This is also verified from SEM-EDAX scans where 7.9 wt% of oxygen and 92.1 wt% of carbon were observed. The presence of surface oxygen, confirmed by EDAX, can be attributed to the oxygen from CO₂ dissociation that possibly got included in the condensed ring aromatic structure in the form of oxygen functionalities. To confirm the nature of oxygen functional groups, FTIR analysis was performed for the carbon samples. Figure 10b shows the FTIR vibrations confirming the presence of cyclic ethers (1140–1070 cm⁻¹), aromatic ethers and

aryl-O stretch ($1270\text{--}1230\text{ cm}^{-1}$), epoxy and oxirane rings peroxides, and C-O-O- stretch ($890\text{--}1250\text{ cm}^{-1}$) [33].

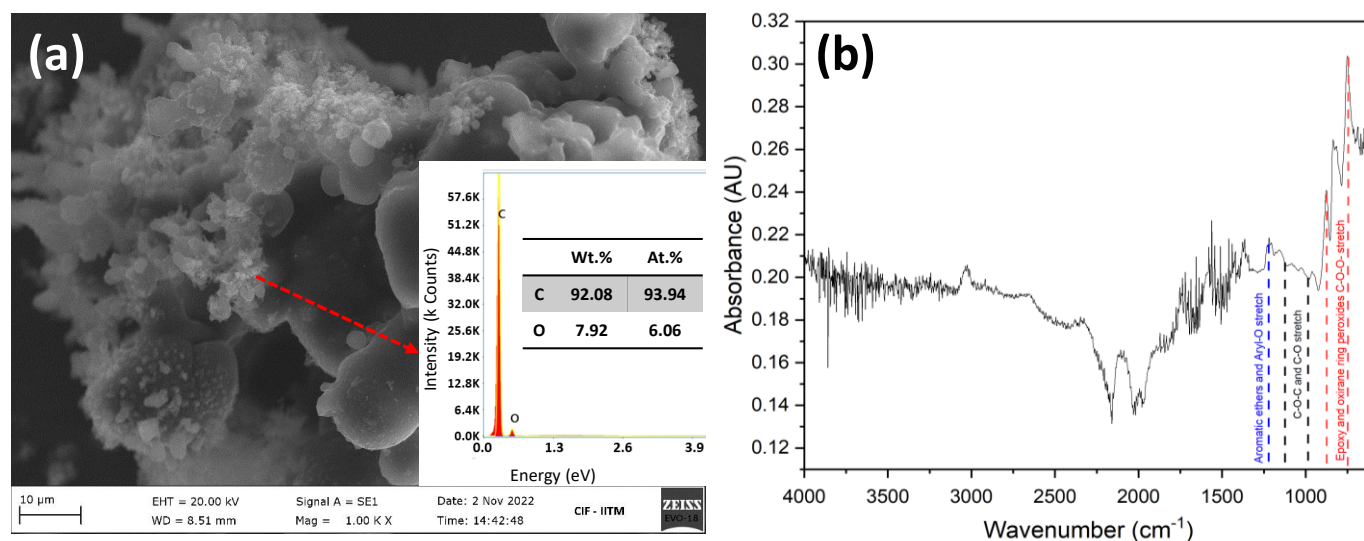


Figure 10. (a) SEM image of the carbon particles collected at 0.5 LPM ($\text{CO}_2\text{:CH}_4$ ratio of 25:75 (v%/v%)). The inset shows the EDAX image and the surface composition of carbon and oxygen. (b) FTIR spectrum of carbon particles.

4. Conclusions

In this first report on dry reforming of methane using a swirl-induced point-plane electrode discharge reactor, the effects of $\text{CO}_2\text{:CH}_4$ composition, flow rate, and power on reactant conversion, product yields, and their composition are thoroughly evaluated. The obtained products include CO, H_2 , and solid carbon along with the production of C_2 hydrocarbons in smaller amounts. At 50 W power, a maximum CO_2 conversion of 23% was obtained at a $\text{CO}_2\text{:CH}_4$ ratio of 75:25 (v%/v%), while a maximum CH_4 conversion of 52% was obtained at a $\text{CO}_2\text{:CH}_4$ ratio of 25:75 (v%/v%). The maximum total conversion of 44% was also achieved with a $\text{CO}_2\text{:CH}_4$ ratio of 25:75 (v%/v%). At 70 W power input, corresponding to 1 LPM flow of the equal composition mixture, the CO_2 conversion, CH_4 conversion, and the total conversion were all 31%, which is significantly higher than that obtained at 50 W. Maximum $\text{H}_2\text{/CO}$ ratios of 5.0–6.0 were recorded for the methane-rich mixtures, i.e., a $\text{CO}_2\text{:CH}_4$ ratio 25:75 (v%/v%), at 1–2 LPM, whereas for all other mixtures the $\text{H}_2\text{/CO}$ ratio was lesser than 2.0. Higher concentrations of the gases at low flow rates enhance the conversion by providing increased availability of molecules and sufficient time for the reaction in the recirculation zones. The results demonstrate that the $\text{H}_2\text{/CO}$ ratio in the product can be regulated by varying the composition of the feed mixture, $\text{CO}_2\text{:CH}_4$, which proves that this technology can be very well applied to the time-varying composition of biogas or landfill gases. The solid carbon nanoparticles were analyzed and were found to be 92% pure with some oxygen on the surface. Although the overall conversion and yield are reasonable in this work, the energy cost is high. The work emphasizes the factors affecting the conversion of reactants and the yield of products, and a suitable reactor configuration for the reaction. With the presented configuration, optimization of SEI can provide better performance at a reduced energy cost.

Author Contributions: Conceptualization, R.B.R., R.S. (Ramanujam Sarathi) and R.V.; Methodology, R.B.R., A.C.H., R.S. (R. Sankar), R.S. (Ramanujam Sarathi) and R.V.; Software, R.S. (Ramanujam Sarathi); Validation, R.B.R. and R.V.; Formal analysis, R.B.R., A.C.H., R.S. (R. Sankar), R.S. (Ramanujam Sarathi) and R.V.; Investigation, R.B.R., A.C.H., R.S. (Ramanujam Sarathi) and R.V.; Resources, R.V.; Data curation, R.B.R. and R.V.; Writing—original draft, R.B.R. and A.C.H.; Writing—review & editing, R.S. (Ramanujam Sarathi) and R.V.; Supervision, R.S. (Ramanujam Sarathi) and R.V.; Funding

acquisition, R.S. (Ramanujam Sarathi) and R.V. All authors have read and agreed to the published version of the manuscript.

Funding: This research received no external funding.

Data Availability Statement: The data presented in this study are available on request from the corresponding author.

Conflicts of Interest: The authors declare no conflict of interest.

References

1. Amponsah, N.Y.; Troldborg, M.; Kington, B.; Aalders, I.; Hough, R.L. Greenhouse Gas Emissions from Renewable Energy Sources: A Review of Lifecycle Considerations. *Renew. Sustain. Energy Rev.* **2014**, *39*, 461–475. [[CrossRef](#)]
2. Li, Y.; Wang, Y.; Zhang, X.; Mi, Z. Thermodynamic Analysis of Autothermal Steam and CO₂ Reforming of Methane. *Int. J. Hydrogen Energy* **2008**, *33*, 2507–2514. [[CrossRef](#)]
3. Qureshi, F.; Yusuf, M.; Kamyab, H.; Zaidi, S.; Junaid Khalil, M.; Arham Khan, M.; Azad Alam, M.; Masood, F.; Bazli, L.; Chelliapan, S.; et al. Current Trends in Hydrogen Production, Storage and Applications in India: A Review. *Sustain. Energy Technol. Assess.* **2022**, *53*, 102677. [[CrossRef](#)]
4. Ekeoma, B.C.; Yusuf, M.; Johari, K.; Abdullah, B. Mesoporous Silica Supported Ni-Based Catalysts for Methane Dry Reforming: A Review of Recent Studies. *Int. J. Hydrogen Energy* **2022**, *47*, 41596–41620. [[CrossRef](#)]
5. Albarazi, A.; Gálvez, M.E.; Da Costa, P. Synthesis Strategies of Ceria–Zirconia Doped Ni/SBA-15 Catalysts for Methane Dry Reforming. *Catal. Commun.* **2015**, *59*, 108–112. [[CrossRef](#)]
6. Pudukudy, M.; Yaakob, Z.; Mohammad, M.; Narayanan, B.; Sopian, K. Renewable Hydrogen Economy in Asia—Opportunities and Challenges: An Overview. *Renew. Sustain. Energy Rev.* **2014**, *30*, 743–757. [[CrossRef](#)]
7. Ranjekar, A.M.; Yadav, G.D. Dry Reforming of Methane for Syngas Production: A Review and Assessment of Catalyst Development and Efficacy. *J. Indian Chem. Soc.* **2021**, *98*, 100002. [[CrossRef](#)]
8. Parsapur, R.K.; Chatterjee, S.; Huang, K.-W. The Insignificant Role of Dry Reforming of Methane in CO₂ Emission Relief. *ACS Energy Lett.* **2020**, *5*, 2881–2885. [[CrossRef](#)]
9. Fridman, A.; Fridman, A.; Kennedy, L.A.; Kennedy, L.A. *Plasma Physics and Engineering*; CRC Press: Boca Raton, FL, USA, 2004; ISBN 978-1-4822-9363-0.
10. Fridman, A.A. *Plasma Chemistry*; Cambridge University Press: Cambridge, UK, 2012; ISBN 978-1-281-38358-7.
11. Tao, X.; Qi, F.; Yin, Y.; Dai, X. CO₂ Reforming of CH₄ by Combination of Thermal Plasma and Catalyst. *Int. J. Hydrogen Energy* **2008**, *33*, 1262–1265. [[CrossRef](#)]
12. Bogaerts, A.; Neyts, E.C. Plasma Technology: An Emerging Technology for Energy Storage. *ACS Energy Lett.* **2018**, *3*, 1013–1027. [[CrossRef](#)]
13. Snoeckx, R.; Zeng, Y.X.; Tu, X.; Bogaerts, A. Plasma-Based Dry Reforming: Improving the Conversion and Energy Efficiency in a Dielectric Barrier Discharge. *RSC Adv.* **2015**, *5*, 29799–29808. [[CrossRef](#)]
14. Raja, R.B.; Sarathi, R.; Vinu, R. Double dielectric barrier discharge-assisted conversion of biogas to synthesis gas. In Proceedings of the 7th International Conference on Advances in Energy Research, Singapore, 18 October 2020; Bose, M., Modi, A., Eds.; Springer Proceedings in Energy; Springer: Singapore, 2021; pp. 123–129, ISBN 9789811559549.
15. Michielsen, I.; Uytendhouwen, Y.; Bogaerts, A.; Meynen, V. Altering Conversion and Product Selectivity of Dry Reforming of Methane in a Dielectric Barrier Discharge by Changing the Dielectric Packing Material. *Catalysts* **2019**, *9*, 51. [[CrossRef](#)]
16. Andersen, J.A.; Christensen, J.M.; Østberg, M.; Bogaerts, A.; Jensen, A.D. Plasma-Catalytic Dry Reforming of Methane: Screening of Catalytic Materials in a Coaxial Packed-Bed DBD Reactor. *Chem. Eng. J.* **2020**, *397*, 125519. [[CrossRef](#)]
17. Uytendhouwen, Y.; Hereijgers, J.; Breugelmans, T.; Cool, P.; Bogaerts, A. How Gas Flow Design Can Influence the Performance of a DBD Plasma Reactor for Dry Reforming of Methane. *Chem. Eng. J.* **2021**, *405*, 126618. [[CrossRef](#)]
18. Chun, S.M.; Hong, Y.C.; Choi, D.H. Reforming of Methane to Syngas in a Microwave Plasma Torch at Atmospheric Pressure. *J. CO₂ Util.* **2017**, *19*, 221–229. [[CrossRef](#)]
19. Xia, Y.; Lu, N.; Wang, B.; Li, J.; Shang, K.; Jiang, N.; Wu, Y. Dry Reforming of CO₂CH₄ Assisted by High-Frequency AC Gliding Arc Discharge: Electrical Characteristics and the Effects of Different Parameters. *Int. J. Hydrogen Energy* **2017**, *42*, 22776–22785. [[CrossRef](#)]
20. Nunnally, T.; Gutsol, K.; Rabinovich, A.; Fridman, A.; Gutsol, A.; Kemoun, A. Dissociation of CO₂ in a Low Current Gliding Arc Plasmatron. *J. Phys. D Appl. Phys.* **2011**, *44*, 274009. [[CrossRef](#)]
21. Ramakers, M.; Trenchev, G.; Heijkers, S.; Wang, W.; Bogaerts, A. Gliding Arc Plasmatron: Providing an Alternative Method for Carbon Dioxide Conversion. *ChemSusChem* **2017**, *10*, 2642–2652. [[CrossRef](#)] [[PubMed](#)]
22. Cleiren, E.; Heijkers, S.; Ramakers, M.; Bogaerts, A. Dry Reforming of Methane in a Gliding Arc Plasmatron: Towards a Better Understanding of the Plasma Chemistry. *ChemSusChem* **2017**, *10*, 4025–4036. [[CrossRef](#)]
23. Slaets, J.; Aghaei, M.; Ceulemans, S.; Van Alphen, S.; Bogaerts, A. CO₂ and CH₄ Conversion in “Real” Gas Mixtures in a Gliding Arc Plasmatron: How Do N₂ and O₂ Affect the Performance? *Green Chem.* **2020**, *22*, 1366–1377. [[CrossRef](#)]

24. Zhang, H.; Li, L.; Li, X.; Wang, W.; Yan, J.; Tu, X. Warm Plasma Activation of CO₂ in a Rotating Gliding Arc Discharge Reactor. *J. CO₂ Util.* **2018**, *27*, 472–479. [[CrossRef](#)]
25. Raja, R.B.; Sarathi, R.; Vinu, R. Development of a Swirl-Induced Rotating Glow Discharge Reactor for CO₂ Conversion: Fluid Dynamics and Discharge Dynamics Studies. *Energy Technol.* **2020**, *8*, 2000535. [[CrossRef](#)]
26. Raja, R.B.; Sarathi, R.; Vinu, R. Selective Production of Hydrogen and Solid Carbon via Methane Pyrolysis Using a Swirl-Induced Point-Plane Non-Thermal Plasma Reactor. *Energy Fuels* **2022**, *36*, 826–836. [[CrossRef](#)]
27. Zhang, X.; Cha, M.S. Electron-Induced Dry Reforming of Methane in a Temperature-Controlled Dielectric Barrier Discharge Reactor. *J. Phys. D Appl. Phys.* **2013**, *46*, 415205. [[CrossRef](#)]
28. Sun, J.; Chen, Q. Kinetic Roles of Vibrational Excitation in RF Plasma Assisted Methane Pyrolysis. *J. Energy Chem.* **2019**, *39*, 188–197. [[CrossRef](#)]
29. Pinhão, N.; Moura, A.; Branco, J.B.; Neves, J. Influence of Gas Expansion on Process Parameters in Non-Thermal Plasma Plug-Flow Reactors: A Study Applied to Dry Reforming of Methane. *Int. J. Hydrogen Energy* **2016**, *41*, 9245–9255. [[CrossRef](#)]
30. Wanten, B.; Maerivoet, S.; Vantomme, C.; Slaets, J.; Trenchev, G.; Bogaerts, A. Dry Reforming of Methane in an Atmospheric Pressure Glow Discharge: Confining the Plasma to Expand the Performance. *J. CO₂ Util.* **2022**, *56*, 101869. [[CrossRef](#)]
31. Wu, A.; Yan, J.; Zhang, H.; Zhang, M.; Du, C.; Li, X. Study of the Dry Methane Reforming Process Using a Rotating Gliding Arc Reactor. *Int. J. Hydrogen Energy* **2014**, *39*, 17656–17670. [[CrossRef](#)]
32. Martin-del-Campo, J.; Coulombe, S.; Kopyscinski, J. Influence of Operating Parameters on Plasma-Assisted Dry Reforming of Methane in a Rotating Gliding Arc Reactor. *Plasma Chem. Plasma Process.* **2020**, *40*, 857–881. [[CrossRef](#)]
33. Coates, J. Interpretation of Infrared Spectra, A Practical Approach. In *Encyclopedia of Analytical Chemistry*; Meyers, R.A., Ed.; John Wiley & Sons, Ltd.: Chichester, UK, 2006; p. a5606. ISBN 978-0-470-02731-8.

Disclaimer/Publisher's Note: The statements, opinions and data contained in all publications are solely those of the individual author(s) and contributor(s) and not of MDPI and/or the editor(s). MDPI and/or the editor(s) disclaim responsibility for any injury to people or property resulting from any ideas, methods, instructions or products referred to in the content.